

Topological property of graphene with triangular array of nanoholes

Yong-Cheng Jiang(江咏城), Xing-Xiang Wang(王星翔), and Xiao Hu(胡晓)

Citation: Chin. Phys. B, 2026, 35 (**5**): 057305. DOI: 10.1088/1674-1056/ae6906
http://cpb.iphy.ac.cn; http://iopscience.iop.org/cpb

What follows is a list of articles you may be interested in

Quantum anomalous Hall effect in twisted bilayer graphene

Wen-Xiao Wang(王文晓), Yi-Wen Liu(刘亦文), and Lin He(何林)
Chin. Phys. B, 2025, 34 (**4**): 047301. DOI: 10.1088/1674-1056/adb38a

Higher-order topology in twisted multilayer systems: A review

Chunbo Hua(花春波) and Dong-Hui Xu(许东辉)
Chin. Phys. B, 2025, 34 (**3**): 037301. DOI: 10.1088/1674-1056/ada885

Field induced Chern insulating states in twisted monolayer-bilayer graphene

Zhengwen Wang(王政文), Yingzhuo Han(韩英卓), Kenji Watanabe, Takashi Taniguchi, Yuhang Jiang(姜宇航), and Jinhai Mao(毛金海)
Chin. Phys. B, 2024, 33 (**6**): 067301. DOI: 10.1088/1674-1056/ad3b8a

Light-modulated graphene-based φ_0 Josephson junction and -φ_0 to φ_0 transition

Renxiang Cheng(程任翔), Miao Yu(于苗), Hong Wang(汪洪), Deliang Cao(曹德亮), Xingao Li(李兴鳌), Fenghua Qi(戚凤华), and Xingfei Zhou(周兴飞)
Chin. Phys. B, 2024, 33 (**2**): 027302. DOI: 10.1088/1674-1056/ad04c5

Tunable Weyl fermions and Fermi arcs in magnetized topological crystalline insulators

Junwei Liu(刘军伟), Chen Fang(方辰), Liang Fu(傅亮)
Chin. Phys. B, 2019, 28 (**4**): 047301. DOI: 10.1088/1674-1056/28/4/047301

LETTER

Topological property of graphene with triangular array of nanoholes

Yong-Cheng Jiang(江咏城)[1,2], Xing-Xiang Wang(王星翔)[1], and Xiao Hu(胡晓)[1,2,†]

[1] *Institute for Quantum Science and Technology, Shanghai University, Shanghai* 200444, *China*
[2] *Department of Physics, College of Sciences, Shanghai University, Shanghai* 200444, *China*

(Received 30 April 2026; accepted manuscript online 6 May 2026)

The nontrivial band topology for graphene with regular arrays of nanoholes with C_{6v} symmetry is investigated theoretically. For the case of the $3\sqrt{3}\times 3\sqrt{3}$ triangular array of nanoholes, we find an energy gap at the Γ point around the Fermi level associated with a band inversion which induces a change in parity indices, whereas deep below the Fermi level there is a bunch of valence bands (VBs) characterized as an obstructed atomic limit (OAL) which also accommodates an imbalance in parity indices. This band structure renders the gap at the Fermi level topologically trivial and carrying no edge states, while the nontrivial band topology of the OAL manifests in two flat bands in the ribbon structure associated with localized electronic states at the ribbon edges. The present results exhibit rich topological behaviors in graphene derivatives waiting for exploration.

Keywords: topological crystalline insulator, graphene derivative, Wannier center, parity index

PACS: 73.22.Pr, 02.40.–k

DOI: 10.1088/1674-1056/ae6906 **CSTR:** 32038.14.CPB.ae6906

1. Introduction

Honeycomb lattices play a special role in fostering topological physics.[1] The Haldane model[2] was defined on a honeycomb lattice where the nearest-neighbor (nn) hopping integrals form the Dirac dispersion, and the complex next-nearest-neighbor (nnn) ones open a gap, establishing a Chern insulator.[3,4] Kane and Mele noticed that, considering the spin degree of freedom, spin–orbit coupling appears associated with the nnn hopping integral, rendering the topological insulator characterized by a Z_2 invariant.[5,6]

A spinless tight-binding (TB) model was proposed on a honeycomb lattice[7,8] where real nn hopping integrals are detuned in a way respecting C_{6v} symmetry, known as the Wu–Hu model.[9,10] When the hopping integral inside a hexagonal unit cell t_0 is smaller than the one between unit cells t_1, namely, $t_1 > t_0$, a topological energy gap $\delta = t_1 - t_0$ is opened in the Dirac dispersions at the Γ point of the Brillouin zone (BZ). The eigen wavefunctions at the upper/lower band edge are p_x & $p_y/d_{x^2-y^2}$ & d_{2xy}. This p–d band inversion induces an imbalance in the parity indices of the valence bands (VBs) between the high-symmetry momenta Γ and M points, yielding nontrivial topology fostered by crystalline symmetry,[11] which can be characterized in terms of Euler class when C_2T symmetry is exploited over the entire BZ.[12–15]

The above physics can be extended to graphene with regular arrays of nanoholes,[16–20] which may be fabricated using bottom-up synthesis methods.[21,22] Generally when $m\sqrt{3}\times m\sqrt{3}$ and $3m\times 3m$ triangular and/or honeycomb array of nanoholes are punctured in graphene, where a nanohole is formed by removing six carbon atoms with appropriate hydrogenation, an energy gap is opened in double Dirac cones at the Fermi level by the intervalley interaction due to the BZ folding.

The topology of a gapped state can be characterized by the localization at non-atomic Wyckoff positions of Wannier functions associated with relevant bands.[23–25] As a matter of fact, topological materials have been diagnosed recently with the aids of material databases[26–29] using topological quantum chemistry[23,24] and symmetry indicators.[30–32]

In this work, we focus on graphene with $3\sqrt{3}\times 3\sqrt{3}$ triangular array of nanoholes. For this system, a topological diagnosis can be performed based on an analysis of Wyckoff positions of Wannier centers directly from the number of VBs modulo six, related to the C_{6v} symmetry, $N_{\rm VB}\pmod 6$.[33] Interestingly, we find topological properties in this system although the diagnosis in terms of $N_{\rm VB}\pmod 6$ suggests a trivial topology at the Fermi level.

2. Tight-binding model

As illustrated in Fig. 1(a), the system studied in this work is formed by introducing a $3\sqrt{3}\times 3\sqrt{3}$ triangular array of nanoholes in graphene, where each nanohole is created by removing six carbon atoms with the perimeter passivated by hydrogen. We denote pristine graphene as the 1×1 structure with its two unit vectors and lattice constant $a_{\rm Gr}$, such that the $3\sqrt{3}\times 3\sqrt{3}$ superstructure denotes that the lattice constants of

†Corresponding author. E-mail: hu_xiao@shu.edu.cn

© 2026 Chinese Physical Society and IOP Publishing Ltd. All rights, including for text and data mining, AI training, and similar technologies, are reserved.

its two unit vectors are $|\boldsymbol{a}_{1,2}|/a_{\rm Gr} = 3\sqrt{3}$. We adopt the following TB Hamiltonian to describe the electronic properties of the π electrons in the superstructured graphene:

$$H = -t\sum_{\langle i,j\rangle} c_i^{\dagger}c_j + \text{H.c.}, \tag{1}$$

where the sites in nanoholes are omitted from the summation and the nn hopping energy $t = 2.7$ eV[3] is assigned to the remaining sites.

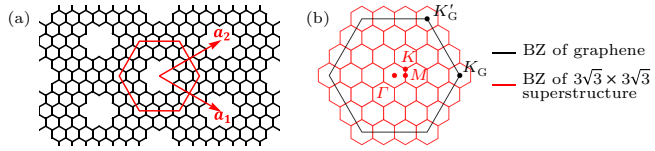


Fig. 1. (a) Schematic structure of graphene with $3\sqrt{3}\times3\sqrt{3}$ triangular array of nanoholes with its unit cell and unit vectors. (b) Brillouin zone (BZ) folding from pristine graphene to graphene with $3\sqrt{3}\times3\sqrt{3}$ superstructure.

3. Results

3.1. Nontrivial topology

The band structure for graphene with $3\sqrt{3}\times3\sqrt{3}$ triangular array of nanoholes calculated by the TB model (1) is shown in Fig. 2(a), where all VBs with parity index[16] at the Γ and M points are displayed explicitly. Near the Fermi level, a large energy gap is opened in the double Dirac cones of pristine graphene, which is induced by intervalley interactions from the BZ folding depicted in Fig. 1(b). The parity indices accumulated for all VBs between the Γ and M points are balanced, namely, $(N_M^+, N_\Gamma^+) = (12, 12)$, indicating trivial topology for the energy gap at the Fermi level. The trivial topology is expected from the 6*d* or 6*e* Wyckoff positions of the Wannier centers since the number of VBs $N_{\rm VB} = (3\sqrt{3})^2 - 3$ modulo six is zero.[33]

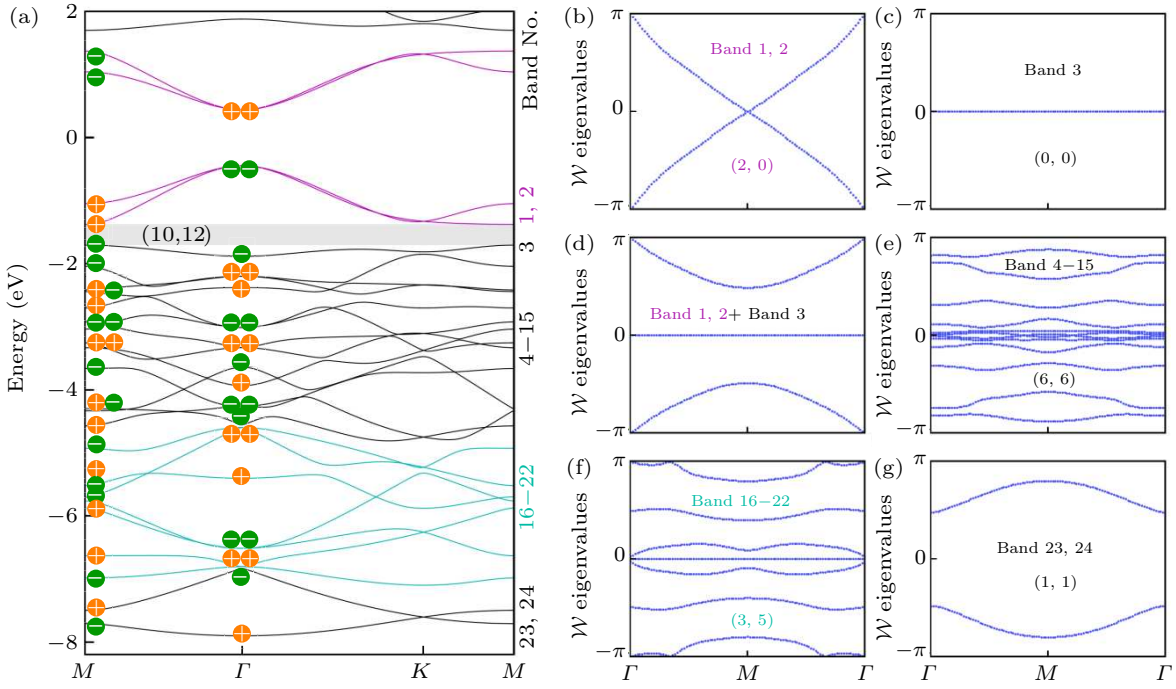


Fig. 2. (a) Band structure with the top two valence bands and band Nos. 16–22 characterized by fragile topology and obstructed atomic limit, respectively. Parity indices at the M and Γ points accumulated below the energy gap in gray are denoted in the bracket. (b)–(g) Eigenvalues of Wilson-loop phases for bands Nos. 1, 2 (b), No. 3 (c), Nos. 1–3 (d), Nos. 4–15 (e), Nos. 16–22 (f), and Nos. 23, 24 (g), parity indices within each set of bands at the M and Γ points are denoted in the bracket.

Interestingly, by further characterizing the topology within the entangled bands below the Fermi level using Wilson loop,[35] we find two sets of bands carrying nontrivial topology, rather than all VBs being topologically trivial. First of all, the eigenvalues of Wilson-loop phases for the top two VBs separated from other bands wind from $-\pi$ to π. This winding, however, is suppressed when the trivial band No. 3 is added as shown in Figs. 2(b)–2(d), indicating fragile topology.[24,36] Bands No. 16 through No. 22 are characterized as an obstructed atomic limit (OAL).[23,37] This is judged from unbalanced parity indices $(N_M^+, N_\Gamma^+) = (3,5)$, while the eigenvalues of Wilson-loop phases show no winding (see Figs. 2(a) and 2(f)). For other VBs, the eigenvalues of Wilson-loop phases display no winding and the parity indices are balanced (see Figs. 2(e) and 2(g)), meaning that these bands are topologically trivial. We notice that graphene with a $3\sqrt{3}\times3\sqrt{3}$ triangular array of nanoholes is a case where VBs exhibit both fragile topology and OAL, and both types of topology may be characterized by a nontrivial Z_2 invariant such that their combination leads to a trivial energy gap at the Fermi level.

The fragile topology and OAL can also be diagnosed from the irreducible representations (irreps) at high-symmetry momenta.[23] In a C_{6v}-symmetric system, the irreps at high-symmetry momenta are summarized in Table A1 in Ap-

pendix A. For the top two VBs, the irreps for the wavefunctions are $(M_1, M_2, \Sigma_1, \Sigma_2, \Gamma_6, K_3)$, as displayed in Fig. 3(a), which characterize fragile topology by matching the difference of two elementary band representations, namely, $(B_1)_{3c} \ominus (B_2)_{1a}$.[24] This band representation indicates an obstruction to constructing exponentially localized Wannier functions while respecting all symmetries of the system. However, after adding a trivial band associated with a localized Wannier orbital B_2 (see its symmetry in the top panel of Table A1 in Appendix A) at the $1a$ Wyckoff position, the resulting three bands can be represented by three localized Wannier orbitals B_1 at the $3c$ Wyckoff positions. For bands No. 16 through No. 22, the irreps for the wavefunctions at the M, Γ, and K points are $(2M_1, M_2, 2M_3, 2M_4, \Gamma_1, 2\Gamma_5, \Gamma_6, 2K_1, K_2, 2K_3)$, as shown in Fig. 3(b), which match the sum of two elementary band representations, namely, $(E)_{2b} \oplus (A_1)_{3c}$.[23] This band representation has localized, symmetric Wannier functions sitting away from atomic sites, and thus its topology is characterized as OAL.[23]

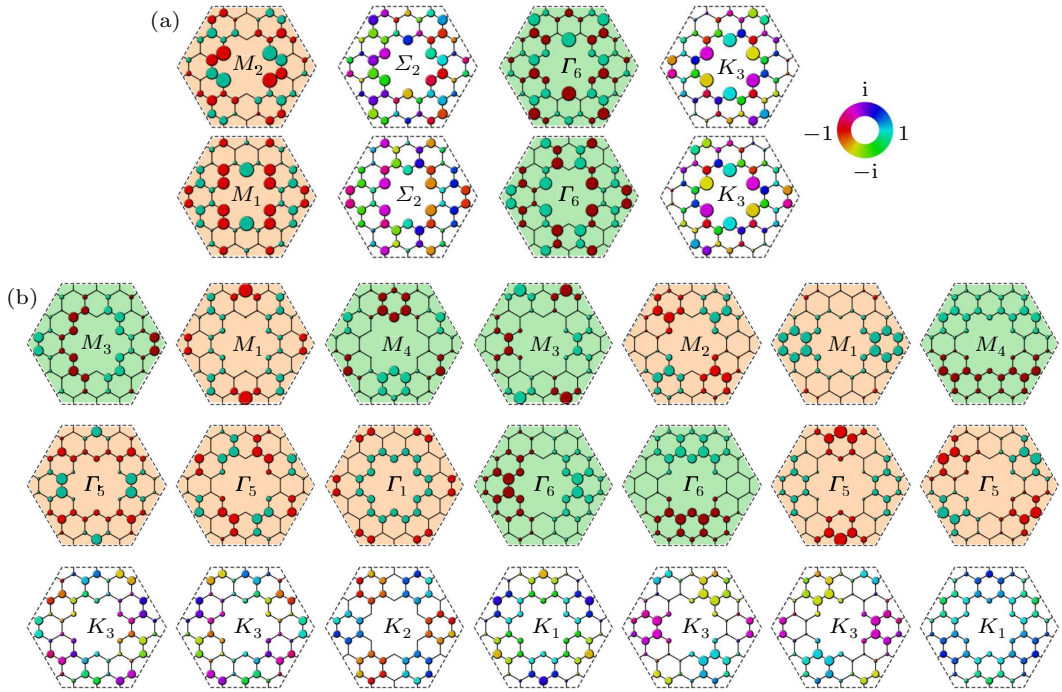


Fig. 3. (a) Wavefunctions of the top two valence bands at the high-symmetric momenta M, Σ, Γ and K. (b) Wavefunctions of bands Nos. 16–22 at the high-symmetric momenta M, Γ and K displayed in the descending order of energy from left to right. The amplitudes and phases of wavefunctions are denoted by size and color of dots, respectively.

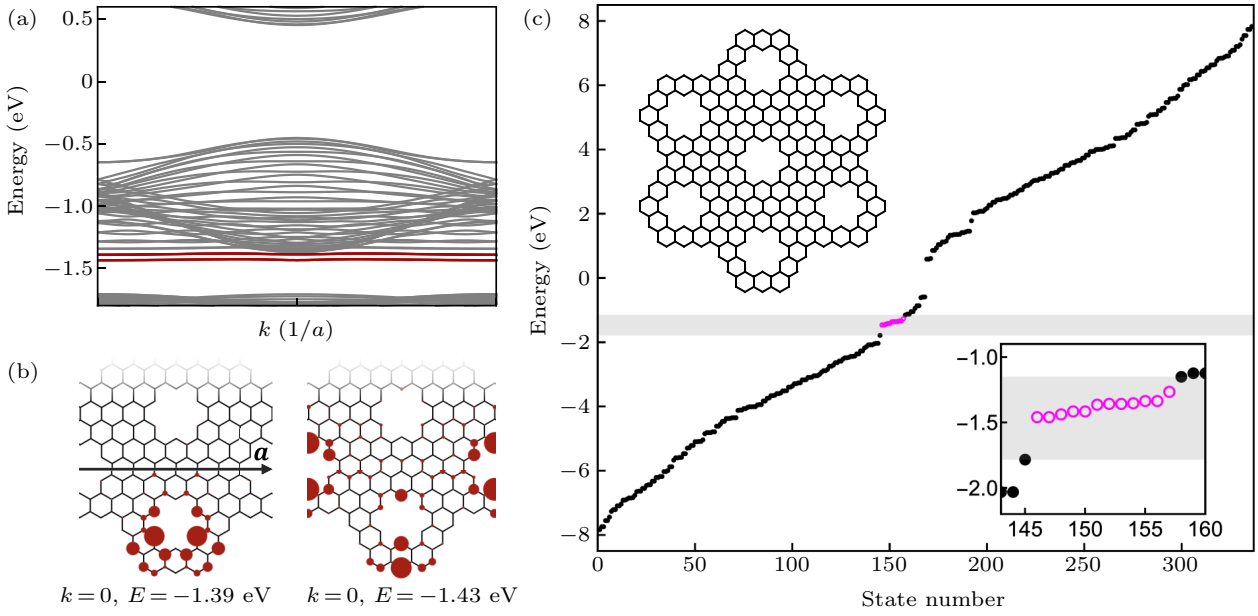


Fig. 4. (a) Energy dispersion of a ribbon structure with the topological band gap denoted by a gray region. (b) Local density of states for the immobile edge states. (c) Energy spectrum of a flake composed of seven unit cells, with edge states (magenta dots) in the energy gap (gray region) around $E = -1.5$ eV. The left inset is the schematic of the flake structure, and the right inset shows an enlarged view of the energy spectrum.

3.2. Topological edge states

We display the energy dispersion for a ribbon structure that is infinitely long in the $\boldsymbol{a} = \boldsymbol{a}_1 + \boldsymbol{a}_2$ direction and is 20 unit cells wide along the $\boldsymbol{a}_2$ direction in Fig. 4(a). Note that the edge morphology of the ribbon is molecular-zigzag,[38] as shown in Fig. 4(b), where hexagonal unit cells remain intact. Two immobile edge states, with their distributions disconnected in the infinite direction as illustrated in Fig. 4(b), appear within a band gap of 0.3 eV near $E = -1.5$ eV (gray region in Fig. 4(a)). The parity indices accumulated for the VBs below this band gap are unbalanced $(N_M^+, N_\Gamma^+) = (10, 12)$, as shown in Fig. 2(a). We can see that the bands of OAL centered at $E = -6$ eV account for the imbalance of parity indices and thus the appearance of edge states in the band gap at $E = -1.5$ eV. In contrast, although the top two VBs are characterized as fragile topology, there is an edge state at the Fermi level given that the parity indices accumulated by all VBs are balanced $(N_M^+, N_\Gamma^+) = (12, 12)$. It is clear that the parity indices dominate the energy at which the edge states appear.

In the flake structure consisting of seven unit cells and respecting C_{6v} symmetry as depicted in the left inset of Fig. 4(c), we also find that the edge states associated with the bands of OAL appear in the energy gap at $E = -1.5$ eV and no edge state exists at the Fermi level, as presented in Fig. 4(c). Note that this flake structure is the smallest one that can host edge states, providing a feasible experimental platform to examine the edge states associated with fragile topology and OAL.

3.3. Design for molecular graphene

As a proof-of-concept experiment, we suggest realizing the flake structure using molecular graphene, which is constructed by aligning CO molecules on a Cu(111) surface with atomic precision using the STM technique.[39] Here we provide the design of molecular graphene with a $3\sqrt{3} \times 3\sqrt{3}$ triangular array of nanoholes, as shown in Fig. 5. The positioning of CO molecules on the Cu(111) surface is displayed schematically in Fig. 5(a), where, besides the CO molecules used to form the hopping pattern (black dots), additional CO molecules are used to block undesired interactions with the surrounding two-dimensional electron gas (gray dots)[40] and to create the effective nanoholes and the edge morphology where all hexagonal unit cells remain intact. The total number of CO molecules used to construct the molecular graphene flake shown in Fig. 5(b) is 306. Because our design structure is smaller than the molecular graphene realized in a recent experiment, where maximally 522 CO molecules were used,[40] the topological electronic states in the graphene flake proposed here are ready to be verified experimentally.

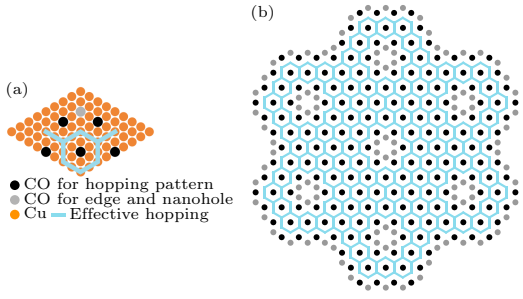


Fig. 5. Schematic for molecular graphene. (a) CO molecules on Cu(111) surface. The CO molecules given by black dots form the effective hopping pattern while the CO molecules given by gray dots form the edge morphology and the nanoholes. (c) Molecular graphene for $3\sqrt{3} \times 3\sqrt{3}$ triangular array of nanoholes, which consists of 306 CO molecules in total.

4. Discussion and conclusion

In order to realize topological states in graphene with superstructures, nanohole arrays should be introduced with atomic precision. Advanced techniques for this purpose include nanoporous graphene and graphene nanoribbons using molecular polymerization,[21,22] helium microscopy[41] and graphene hydrogenation.[42,43] Chemical synthesis based on precursors with heteroatoms[44] is also promising. While in the present work we focus explicitly on graphene, the scheme conceived here is applicable to other Dirac materials, with honeycomb-patterned GaAs quantum wells[45] as a promising candidate.

To summarize, we theoretically investigate the nontrivial band topology for graphene with regular arrays of nanoholes with C_{6v} symmetry, where an energy gap is opened at the Γ point of the Brillouin zone due to intervalley interactions associated with Brillouin zone folding from pristine graphene. In particular, for the case of a $3\sqrt{3} \times 3\sqrt{3}$ triangular array of nanoholes, which are formed by removing six carbon atoms, we find a large energy band gap at the Γ point at the Fermi level and a band inversion between bands of opposite parities. In contrast to the simplest consideration based on the two bands close to the Fermi level, no topological edge states can be observed. To understand this behavior, we analyze the full set of valence bands and find that, in addition to the above band inversion at the Fermi level, there is a set of valence bands much below the Fermi level characterized by OAL which also accommodates an imbalance in parity indices. Therefore, the two top valence bands can be considered as having fragile topology carrying no topological edge states. It is revealed that the nontrivial band topology of the OAL manifests in two flat bands in the ribbon structure associated with localized electronic states at the ribbon edges. The present results exhibit rich topological behaviors in graphene derivatives awaiting experimental exploration and are potentially useful for electronic device applications.

Appendix A

Character tables and irreps for point groups at high-symmetric momenta in a C_{6v}-symmetric system are presented in Table A1.

Table A1. Irreps at high-symmetric momenta for a C_{6v}-symmetric system. Top panel: character tables for C_{6v}, C_{3v}, C_{2v} and C_s point groups, with standard notations of irreps[46] in the first column and notations of irreps at the Γ, K, M and Σ[47] in the second column. Bottom panel: all possible irreps along the mirror-symmetric line Σ in BZ at high-symmetric momenta for the two bands with degenerate states at the Γ point in a C_{6v}-symmetric system.[48]

C_{6v}		E	C_2	$2C_3$	$2C_6$	$3\sigma_d$	$3\sigma_v$
A_1	Γ_1	1	1	1	1	1	1
A_2	Γ_2	1	1	1	1	−1	−1
B_2	Γ_3	1	−1	1	−1	1	−1
B_1	Γ_4	1	−1	1	−1	−1	1
E_2	Γ_5	2	2	−1	−1	0	0
E_1	Γ_6	2	−2	−1	1	0	0

C_{3v}		E	$2C_3$	$3\sigma_v$
A_1	K_1	1	1	1
A_2	K_2	1	1	−1
E	K_3	2	−1	0

C_{2v}		E	C_2	σ_v	σ'_v
A_1	M_1	1	1	1	1
A_2	M_2	1	1	−1	−1
B_2	M_3	1	−1	−1	1
B_1	M_4	1	−1	1	−1

C_s		E	σ_v
A'	Σ_1	1	1
A''	Σ_2	1	−1

Momentum	Γ	K	M	Σ
Site symmetry	C_{6v}	$\mathcal{M}$	C_{2v}	C_{3v}
Irreducible representation	E_1	$A'+A''$	A_1+A_2	E
	E_2		A_1+B_2	A_1+A_2
			B_1+A_2	
			B_1+B_2	

Acknowledgments

The authors are grateful to T. Kariyado for valuable discussions. Project supported by Shanghai Science and Technology Innovation Action Plan (Grant No. 24LZ1400800).

References

[1] Klitzing K V, Dorda G and Pepper M 1980 *Phys. Rev. Lett.* **45** 494
[2] Haldane F D M 1988 *Phys. Rev. Lett.* **61** 2015
[3] Thouless D J, Kohmoto M, Nightingale M P and den Nijs M 1982 *Phys. Rev. Lett.* **49** 405
[4] Weng H, Yu R, Hu X, Dai X and Fang Z 2015 *Adv. Phys.* **64** 227
[5] Kane C L and Mele E J 2005 *Phys. Rev. Lett.* **95** 226801
[6] Kane C L and Mele E J 2005 *Phys. Rev. Lett.* **95** 146802
[7] Wu L H and Hu X 2015 *Phys. Rev. Lett.* **114** 223901
[8] Wu L H and Hu X 2016 *Sci. Rep.* **6** 24347
[9] Leykam D, Xue H, Zhang B and Chong Y D 2017 *Opt. Lett.* **8** 55
[10] Zhu B, Liu H, Wang Q, Chong Y D and Wang Q J 2019 *Phys. Rev. B* **100** 214301
[11] Fu L 2011 *Phys. Rev. Lett.* **106** 106802
[12] Palmer S J and Giannini V 2018 *New J. Phys.* **3** L022013
[13] Wang X X, Kariyado T and Hu X 2018 *Phys. Rev. B* **134** 099301
[14] Ahn J, Park S, Kim D, Kim Y and Yang B J 2019 *Phys. Rev. B* **28** 117101
[15] Wang K, Dai J X, Shao L, Yang S A and Zhao Y 2020 *Phys. Rev. Lett.* **125** 126403
[16] Kariyado T, Jiang Y C, Yang H and Hu X 2018 *Phys. Rev. B* **98** 195416
[17] Zhao J, Ji P, Li Y, Li R, Zhang K, Tian H, Yu K, Bian B, Hao L, Xiao X, Griffin W, Dudeck N, Moro R, Ma L and de Heer W A 2023 *Nature* **625** 60
[18] Shima N and Aoki H 1993 *Phys. Rev. B* **71** 4389
[19] Pedersen T G, Flindt C, Pedersen J, Mortensen N A, Jauho A P and Pedersen K 2008 *Phys. Rev. Lett.* **100** 136804
[20] Bai J, Zhong X, Jiang S, Huang Y and Duan X 2010 *Nat. Nanotechnol.* **5** 190
[21] Moreno C, Vilas-Varela M, Kretz B, *et al.* 2018 *Science* **360** 199
[22] Song S, Teng Y, Tang W, Xu Z, He Y, Ruan J, Kojima T, Hu W, Giessibl F J, Sakaguchi H, Louie S G and Lu J 2022 *Nature* **637** 580
[23] Bradlyn B, Elcoro L, Cano J, Vergniory M G, Wang Z, Felser C, Aroyo M I and Bernevig B A 2017 *Nature* **547** 298
[24] Cano J, Bradlyn B, Wang Z, Elcoro L, Vergniory M G, Felser C, Aroyo M I and Bernevig B A 2018 *Phys. Rev. Lett.* **120** 266401
[25] Marzari N, Mostofi A A, Yates J R, Souza I and Vanderbilt D 2012 *Rev. Mod. Phys.* **84** 1419
[26] Zhang T, Jiang Y, Song Z, Huang H, He Y, Fang Z, Weng H and Fang C 2019 *Nature* **566** 475
[27] Vergniory M G, Elcoro L, Felser C, Regnault N, Bernevig B A and Wang Z 2019 *Nature* **566** 480
[28] Tang F, Po H C, Vishwanath A and Wan X 2019 *Nature* **566** 486
[29] Tang F, Po H C, Vishwanath A and Wan X 2019 *Nat. Phys.* **15** 470
[30] Po H C, Vishwanath A and Watanabe H 2017 *Nat. Commun.* **8** 50
[31] Slager R J, Mesaros A, Juričić V and Zaanen J 2013 *Nat. Phys.* **9** 98
[32] Kruthoff J, De Boer J, Van Wezel J, Kane C L and Slager R J 2017 *Phys. Rev. X* **7** 041069
[33] Jiang Y C, Wang X X and Hu X 2026 arXiv:2605.14436
[34] Castro Neto A H and Guinea F 2007 *Phys. Rev. B* **75** 045404
[35] Yu R, Qi X L, Bernevig A, Fang Z and Dai X 2011 *Phys. Rev. B* **84** 075119
[36] Po H C, Watanabe H and Vishwanath A 2018 *Phys. Rev. Lett.* **121** 126402
[37] de Paz M B, Vergniory M G, Bercioux D, García-Etxarri A and Bradlyn B 2019 *Phys. Rev. Res.* **1** 032005
[38] Kariyado T and Hu X 2017 *Sci. Rep.* **7** 16515
[39] Gomes K K, Mar W, Ko W, Guinea F and Manoharan H C 2012 *Nature* **483** 306
[40] Freeney S E, van den Broeke J J, Harsveld van der Veen A J J, Swart I and Morais Smith C 2020 *Phys. Rev. Lett.* **124** 236404
[41] Nakaharai S, Iijima T, Ogawa S, Suzuki S, Li S L, Tsukagoshi K, Sato S and Yokoyama N 2013 *ACS Nano* **7** 5694
[42] Balog R, Jørgensen B, Nilsson L, *et al.* 2010 *Nat. Mater.* **9** 315
[43] Chen H, Bao D L, Wang D, Que Y, Xiao W, Qian G, Guo H, Sun J, Zhang Y Y, Du S, Pantelides S T and Gao H J 2018 *Adv. Mater.* **30** 1801838
[44] Kawai S, Nakatsuka S, Hatakeyama T, Pawlak R, Meier T, Tracey J, Meyer E and Foster A S 2018 *Sci. Adv.* **4** eaar7181
[45] Wang S, Scarabelli D, Du L, Kuznetsova Y Y, Pfeiffer L N, West K W, Gardner G C, Manfra M J, Pellegrini V, Wind S J and Pinczuk A 2018 *Nat. Nanotechnol.* **13** 29
[46] Mulliken R S 1933 *Phys. Rev.* **43** 279
[47] Elcoro L, Bradlyn B, Wang Z, Vergniory M G, Cano J, Felser C, Bernevig B A, Orobengoa D, de la Flor G and Aroyo M I 2017 *J. Appl. Crystallogr.* **50** 1457
[48] Sakoda K 2005 *Optical Properties of Photonic Crystals* (Berlin: Springer)